ARTICLE OPEN

Check for updates

Strenuous exercise-tolerance stretchable dry electrodes for continuous multi-channel electrophysiological monitoring

Ruijie Xie[1,2,3], Qingsong Li[1], Lijun Teng[1], Zhengshuai Cao[4], Fei Han[1], Qiong Tian[1], Jing Sun[1,5], Yang Zhao[1], Mei Yu[1], Dianpeng Qi[5], Peizhi Guo[4], Guanglin Li[1]✉, Fengwei Huo[2,3]✉ and Zhiyuan Liu[1]✉

Electrophysiological monitoring under strenuous exercise by using stretchable dry electrodes is vital for healthcare monitoring, prosthetic control, human−machine interfaces and other biomedical applications. However, the existing dry electrodes are not applicable to the strenuous exercise situation that always involves both fast moving and profuse sweating. Herein, we present a nano-thick porous stretchable dry electrode system with high stretchability and water permeability. The system attaches conformably to the skin and stretches with it under Van der Waals forces even at sweating conditions, allowing the detection of electromyogram when moving with an acceleration of 10 g at a sweating rate of 2.8 mg cm^{-2} min^{-1}. It is also capable of acquiring electrocardiogram and electroencephalogram signals. The strategy proposed would enable the biomedical studies and related applications with the requirement of stably recording electrophysiological signals under strenuous exercise scenarios.

npj Flexible Electronics (2022)6:75 ; https://doi.org/10.1038/s41528-022-00209-0

INTRODUCTION

Human physiological activities are accompanied by a variety of electrical signals known as electrophysiological signals (EP), such as electromyogram (EMG), electrocardiogram (ECG), and electroencephalogram (EEG)[1–3]. Daily monitoring of these signals has drawn a great deal of attention as it has important applications in the fields of healthcare monitoring[4,5], prosthetic control[6–8], and human−machine interfaces[9,10]. These biomedical applications inevitably involve strenuous exercise, which will cause the skin to undergo violent disturbance and sweat, bringing challenge to the stable acquisition of EP signals.

The commonly used electrodes for EP signal monitoring during sports include gel electrodes and dry electrodes[11,12]. As dehydration and skin irritation occur after the long-term use of gel electrodes[13,14], dry electrodes have emerged as promising alternatives. Many efforts have been devoted to improving the performance of dry electrodes in case of exercise and sweating respectively[15–23]. a. For exercising purpose, ultrathin electrodes, microstructured electrodes, and in-situ formed electrodes with improved anti-motion artifact performance have been demonstrated by enhancing electrode−skin adhesion[24–29]. Takao Someya's group fabricated sub-300 nm dry thin-film electrodes to realize motion artifact-less monitoring of EP signals with skin vibrations of up to 15 μm, as the electrodes were self-adhesive and conformable to complex 3D biological surfaces[30]. Seokwoo Jeon's group combined a gecko-inspired microstructure with a dry electrode to increase the adhesive force with skin, thereby measuring biosignals during wrist curl, squat, and writing[31]. In addition, the in-situ formed electrode on the skin was realized by Cunjiang Yu's group, which could work normally under stretching[32]. b. For application in sweating situation, porosity was introduced to improve the water vapor permeability of the electrode. Porous film[33–35], leather[36], textile[37], and electro spinning mat[38,39] have been used as substrates to fabricate gas permeable electrodes. However, the existing dry electrodes are not applicable to the strenuous exercise situation that always involves both fast moving and profuse sweating (Supplementary Table 1). Therefore, it is still desired to develop a dry electrode system with both good strenuous moving-tolerance and anti-perspiration to monitor physiological electrical signals in actual scenes.

When doing strenuous exercise, human skin would undergo dynamic movement (acceleration, deceleration, stretching, and vibration) and sweating. To achieve stable monitoring of EP signals, the electrode should form a stable interface with the skin[40]. Thus, the desired electrode should adhere well to the skin and stretch with it during body movement. Furthermore, the accumulation of sweat between the electrode and the skin will not only induce discomfort and even skin inflammation but also has an influence on the stability of the electrode−skin interface. As a result, high porosity should also be concerned when designing such electrodes.

Herein, we report a porous nano-thick stretchable dry electrode system to reliably monitor EP signals under strenuous exercise. The porous nano-thick stretchable film is prepared by a one-step method based on Marangoni effect. It shows stretchability of 120% and permeability of 25.3 g m^{-2} h^{-1}, offering skin comfort even under vigorous sweating conditions. The acceleration and sweating rate of limbs are used to evaluate the electrode's performance. The electrode can detect EMG signals when the subject swings his arm with an acceleration of 10 g at a sweating rate of 2.8 mg cm^{-2} min^{-1}. Furthermore, ECG and EEG signals are also acquired when the subject sweats at a rate of 3.2 mg cm^{-2} min^{-1} and 2.6 mg cm^{-2} min^{-1} respectively. The electrode array with proper wire bonding design is successfully

[1]CAS Key Laboratory of Human-Machine Intelligence-Synergy Systems, Shenzhen Institutes of Advanced Technology, Chinese Academy of Sciences (CAS), Shenzhen 518055, China. [2]The Institute of Flexible Electronics (IFE, Future Technologies), Xiamen University, Xiamen, 361005 Fujian, China. [3]Key Laboratory of Flexible Electronics (KLOFE), School of Flexible Electronics (Future Technologies), Nanjing Tech University, 30 South Puzhu Road, Nanjing 211816, China. [4]Institute of Materials for Energy and Environment, State Key Laboratory of Bio-fibers and Eco-textiles, College of Materials Science and Engineering, Qingdao University, Qingdao 266071, China. [5]MIIT Key Laboratory of Critical Materials Technology for New Energy Conversion and Storage, School of Chemistry and Chemical Engineering, Harbin Institute of Technology, Harbin 150001, China.
✉email: gl.li@siat.ac.cn; iamfwhuo@njtech.edu.cn; zy.liu1@siat.ac.cn

fabricated to monitor multi-channel EMG continuously. Thus, the proposed strategy will undoubtedly promote the development of high-performance dry electrodes for biomedical applications and enables the biomedical studies and related applications with the requirement of stably recording electrophysiological signals under strenuous exercise scenarios.

RESULTS AND DISCUSSION

Strategy to fabricate the ultrathin porous electrode

The porous 200 nm-thick stretchable electrode with good strenuous exercise-tolerance and anti-perspiration properties (Fig. 1a) was fabricated by magnetron sputtering a layer of gold on a porous ultrathin stretchable film. As shown in Fig. 1b, the ultrathin porous stretchable film was achieved through a one-step method. By dropping polystyrene-block-poly(ethylene-ran-butylene)-block-polystyrene (SEBS) solution on the surface of water, an ultrathin layer of SEBS solution was formed due to its lower surface tension than water. As toluene evaporated, the concentration of SEBS increased, leading to the decrease of its surface tension and increase of its viscosity (Supplementary Fig. 1). According to the Marangoni effect[41,42], the transport of SEBS solution arising from the change of its surface tension would induce the formation of pores on the film, while the increase of its viscosity would restrict its flowing and limit pore increase. After the toluene was completely evaporated, an ultrathin porous film was achieved. The proposed method involves no equipment and takes less than 30 s to obtain the ultrathin porous stretchable film. To the best of our knowledge, the obtained electrode exhibits the highest stretchability for nano-thick electrode (Fig. 1c) and the best strenuous exercise-tolerance and anti-perspiration performances among those reported in the literature (Fig. 1d).

Components of the electrode system

The electrode with strenuous exercise-tolerance consists of a stable electrode−skin interface and a stable electrode−connecter interface. As shown in Fig. 2a, the electrodes with thicknesses of 200 nm and 5 μm adhere conformably to the skin under Van der Waals forces. Generally, the force used to stretch electrode increases with the electrode thickness, (Fig. 2b), causing different changes of electrode−skin interfaces upon dynamically stretching the skin from 0 to 14% for 100 cycles. Specifically, the adhering force between the 200 nm-thick electrode and the skin is $1.28 \pm 0.08\ cm^{-2}$, which is comparable with other dry electrodes reported earlier[31,43–46]. (Supplementary Table 2) Applying such force, the ultrathin electrode will stretch with the skin and the skin texture is well kept after the stretching process. While for the 5 μm-thick electrode, the higher stretching force drives it to slip from the skin during the process, with bubbles appearing between the electrode and the skin. For this basis, the baseline of EMG signals collected by the 200 nm-thick electrode shows higher stability than those by the thicker electrodes (Fig. 2c). To monitor physiological electrical signals, the ultrathin porous stretchable electrode should to be connected with signal acquisition equipment. As shown in Fig. 2d, flexible conductive medical dressing is used as transition material to connect the ultra-flexible and stretchable electrode with stiff equipment because of its flexibility and breathability. The conductive medical dressing connected with a flexible printed circuit board through anisotropic conductive films is attached to the skin firstly, and then the ultrathin flexible electrode connects the skin and the conductive medical dressing through Van der Waals forces (Fig. 2e). These two stable interfaces guarantee the sensing capability of the electrode during strenuous exercise.

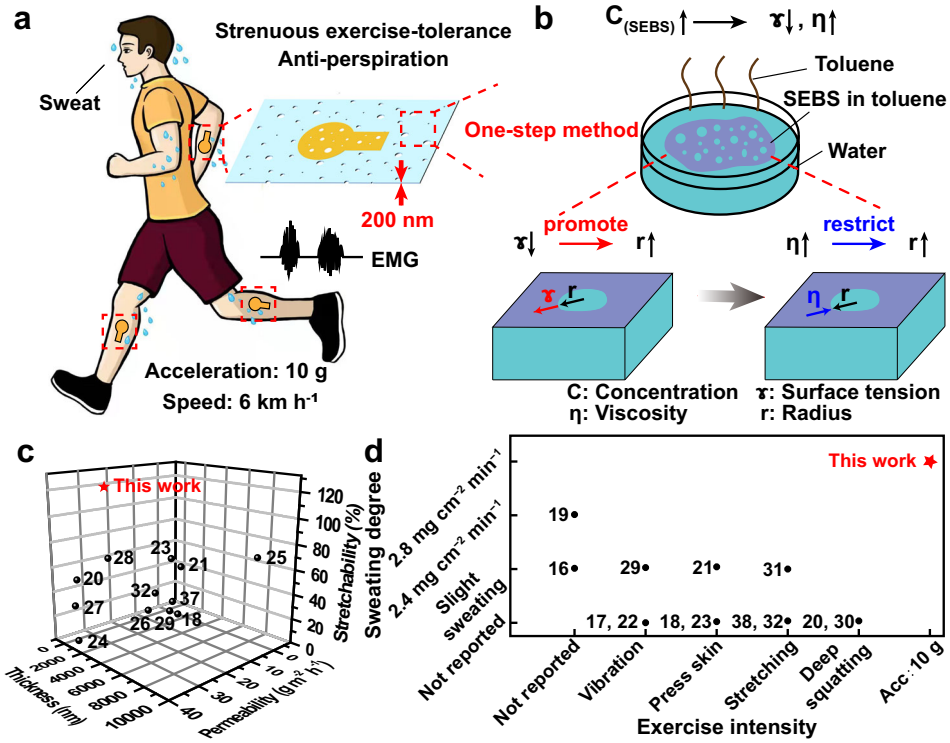

Fig. 1 Features and superiorities of the electrode. a Schematic illustration showing the ultrathin porous stretchable electrode with good strenuous exercise-tolerance and anti-perspiration properties. **b** Fabrication process of the ultrathin porous stretchable film depending on the Marangoni effect. **c** Thickness, permeability, and stretchability comparison between the electrodes reported in the literature and the one in this work. **d** Comparison of the strenuous exercise-tolerance and anti-perspiration between the electrodes reported in the literature and the one in this work.

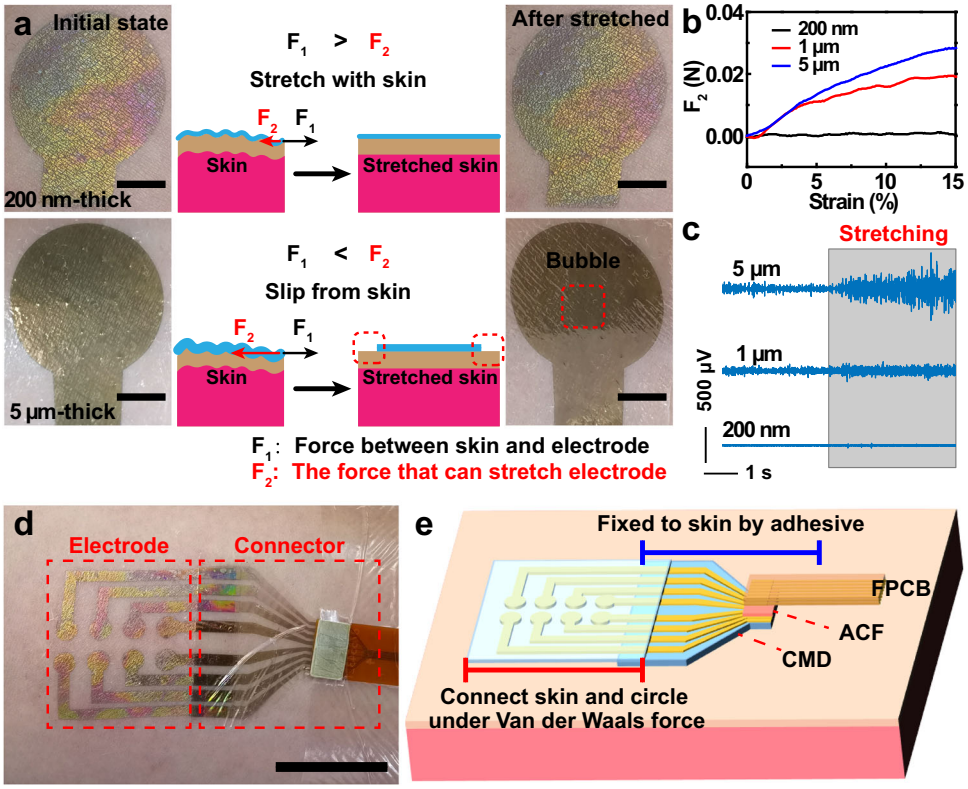

Fig. 2 Reasons for electrode stability. a Electrode−skin interface stability of the electrodes with different thicknesses after the interfaces were stretched for 100 cycles. Scale bar: 5 mm. **b** Forces used to stretch electrodes with different thicknesses. **c** Change of baseline of EMG when the electrode−skin interfaces were stretched for electrodes with different thicknesses. **d** Connection of the electrode with the signal acquisition equipment. Scale bar: 2 cm. **e** Schematic illustration showing the formation process of the connector. FPCB flexible printed circuit board, ACF anisotropic conductive films, CMD conductive medical dressing.

Fabrication of the nano-thick porous stretchable film

The formation of SEBS-based ultrathin porous stretchable film can be divided into two stages: the spread of SEBS solutions on the surface of water and the evaporation of toluene to form porous SEBS film. During the process, three factors, including surface tension of water, concentration of SEBS, and evaporation rate of toluene, may affect the fabrication of ultrathin porous film. The surface tension of water could affect the spread of SEBS solution on its surface. By adjusting the concentration of NaCl in water, water with different surface tensions is obtained (Supplementary Fig. 2). Supplementary Fig. 3a and b shows uneven spread of SEBS solution and inhomogeneous thickness of the formed SEBS film (an error bar of 389.7 nm) under low surface tension of water (deionized water). With the increase of surface tension of water, even spread of SEBS solution is gradually observed on water surface, with the thickness of SEBS film being decreased and more homogenous (an error bar of 21 nm) (Supplementary Fig. 3c–f). When the concentration of NaCl becomes higher than 5 wt%, no obvious variation is observed for the spread area of SEBS solution and the thickness of SEBS film. Consequently, the NaCl solution with a concentration of 5 wt% was adopted to fabricate the SEBS-based ultrathin porous film.

The higher the concentration of SEBS, the higher the viscosity of SEBS solution. As shown in Fig. 3a, the spread area decreases accordingly with the increasing concentration of SEBS solution, resulting in thickness increase of SEBS film. The thicknesses of SEBS films vary from 22 to 790 nm as the concentrations of SEBS increase from 1 to 11 wt%, which also reflected by the structure colors in Supplementary Fig. 4. For SEBS films that thickness less than 100 nm, the mechanical properties were too poor to achieve freestanding film. The freestanding thinnest SEBS film could be achieved by this method was about 100 nm (Fig. 3b, c).

According to the Marangoni effect, the evaporation of toluene would induce (i) the surface tension of SEBS solution to decrease, leading to the flowing of SEBS solution and formation of pores; (ii) the viscosity of SEBS solution to increase, which can be used to evaluate the flowing duration of SEBS solution, and further determine the pore radius of SEBS film. For example, when the evaporation rate is low (0.8 mg cm^{-2} min^{-1}), the viscosity would increase slowly, resulting in long flowing duration of SEBS solution. Finally, a fishnet-like film with pore diameter ranging from 400 to 1000 μm is obtained (Fig. 3d). A further increase in the evaporation rate to 1.4 mg cm^{-2} min^{-1} fastens the increasing rate of viscosity and shortens the flowing duration of SEBS solution. The resulting SEBS film presents decreased pore diameter from 50 to 110 μm (Fig. 3e). However, when we continued to increase the evaporation rate to 8 mg cm^{-2} min^{-1}, an SEBS film with no pores is formed (Fig. 3f). Therefore, the pore diameter is adjustable by tuning the toluene volatilization rate. It should be noted that although SEBS-based films with thicknesses from 45 nm to 800 nm can also be achieved by spin coating method, their pores are hardly regulated (Supplementary Fig. 5). In this respect, our proposed strategy possesses irreplaceable advantage when compared with conventional method.

Stretchability of the ultrathin porous electrode

To fabricate the SEBS-based ultrathin porous electrode, a layer of gold was magnetron sputtered on the SEBS-based ultrathin porous film. Considering the mechanical properties of SEBS film, the one with thickness of 200 nm and pore radius of 50−110 μm was adopted to fabricate the electrode. Typically, the electrode

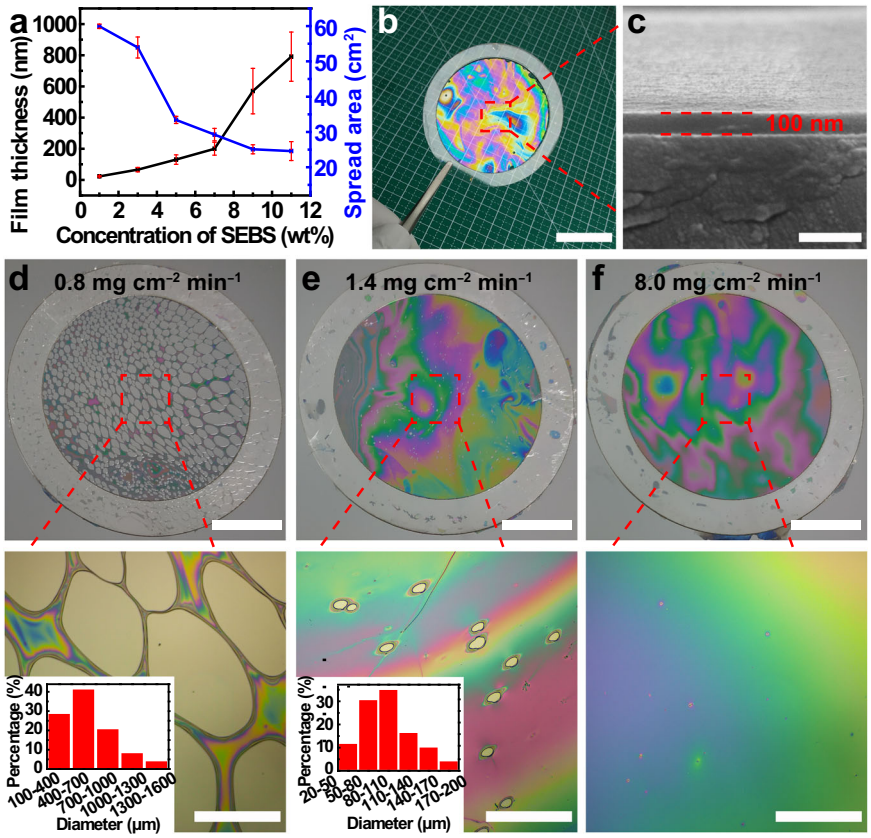

Fig. 3 Fabrication of the ultrathin porous film. a Spread area and thickness of SEBS when 20 μL SEBS solutions with different concentrations being dropped on the surface of water. **b** Photograph of a freestanding SEBS film with thickness of 100 nm. Scale bar: 2 cm. **c** SEM image of the cross section of the SEBS film. Scale bar: 300 nm. **d**–**f** SEBS films formed under different evaporation rates of toluene. Scale bars in low magnification graph: 1 cm; Scale bars in high magnification graph: 500 μm.

would undergo stretching during exercise. The electric characteristic of the electrode was recorded during the stretching process. It can be observed form Supplementary Fig. 6a, the electrode possesses a rough surface. Before stretching process, no microcracks were observed. As shown in Fig. 4a, microcracks appear on the gold layer to keep the electrode conductive under stretching. The thickness of gold layer has a significant influence on the formation of microcracks. Supplementary Fig. 7 discloses that the stretchability of the electrode increases first with the increasing thickness of the gold layer, and then to a certain degree decreases. At the gold layer thickness of 17 nm, the optimal stretchability of the electrode approaches 120% (Fig. 4b). When the electrode was stretched to 120%, the microcracks were too big to keep the conductive pathway connected. Thus, the electrode shows higher resistance. A stable electrode−skin impedance is also vital to the detection of physiological electrical signals during exercise. Two circular ultrathin electrodes with diameter of 1.5 cm were placed on subject' forearm and the distance between the two electrodes was 10 cm. Then, the electrode−skin impedance was measured under different degrees of stretching. As shown in Fig. 4c, no obvious variation of impedance was observed when the skin is stretched from 0% to 14%. High-density EMG can provide more information about muscle and nerve for muscle function evaluation[47,48]. To fabricate high-density electrode, it is necessary to encapsulate the electrode for exposing desired sensing sites. As shown in Supplementary Fig. 8, taking advantage of SEBS's self-adhesiveness, the encapsulation of the electrode was realized by laminating a non-porous SEBS ultrathin film on the electrode. The filter paper possesses low force with the SEBS film, and can be peeled off from the SEBS film. During the encapsulation of the electrodes, a paper sheet was placed between the electrodes and the SEBS film. After removing the filter paper, the sensing sites were exposed. Finally, the electrode was tested for multi-stretching cycles to examine its stability. After being stretched to 30% for 1000 cycles, the electrode maintains low resistance and good stretchability (Fig. 4e), suggesting reliable stability of the as-prepared ultrathin porous stretchable electrode.

EMG recording properties of the electrode system

The ultrathin electrode demonstrates comparable performance to the commercial gel electrode in detecting EMG signals. As shown in Supplementary Figs. 9 and 10a, EMG signals from brachioradialis can be distinguished by the SEBS-based ultrathin electrode when the subject makes different hand gestures or clenches fist with different strengths, even though its impedance is higher (Supplementary Fig. 11), and its signal to noise ratio was lower (Supplementary Fig. 10b) than gel electrode. Under strenuous exercise, the performance of the electrode was further explored. The high-density EMG electrode with 8 channels works normally when the skin is stretched dynamically from 0 to 14% (Fig. 5a and b). Under other conditions, such as swinging the arm with an acceleration of 2 g (Fig. 5c and d), pressing the skin around the electrode, pressing the electrode, vibrating the skin, and twisting the arm, EMG signals are also obtained successfully (Supplementary Movie 1). To validate the performance of the ultrathin dry electrode, more vigorous exercise was conducted. It was laminated on leg to detect EMG during running (Fig. 5e). As shown in Fig. 5f, the running process could be divided into three steps: leg raising off the ground, leg hanging in the air, leg landing on the ground. The biggest acceleration generates in the second state. At a running speed of 3 km h^{-1}, the highest acceleration is ~6 g, and the ultrathin dry electrode shows comparable performance to the gel

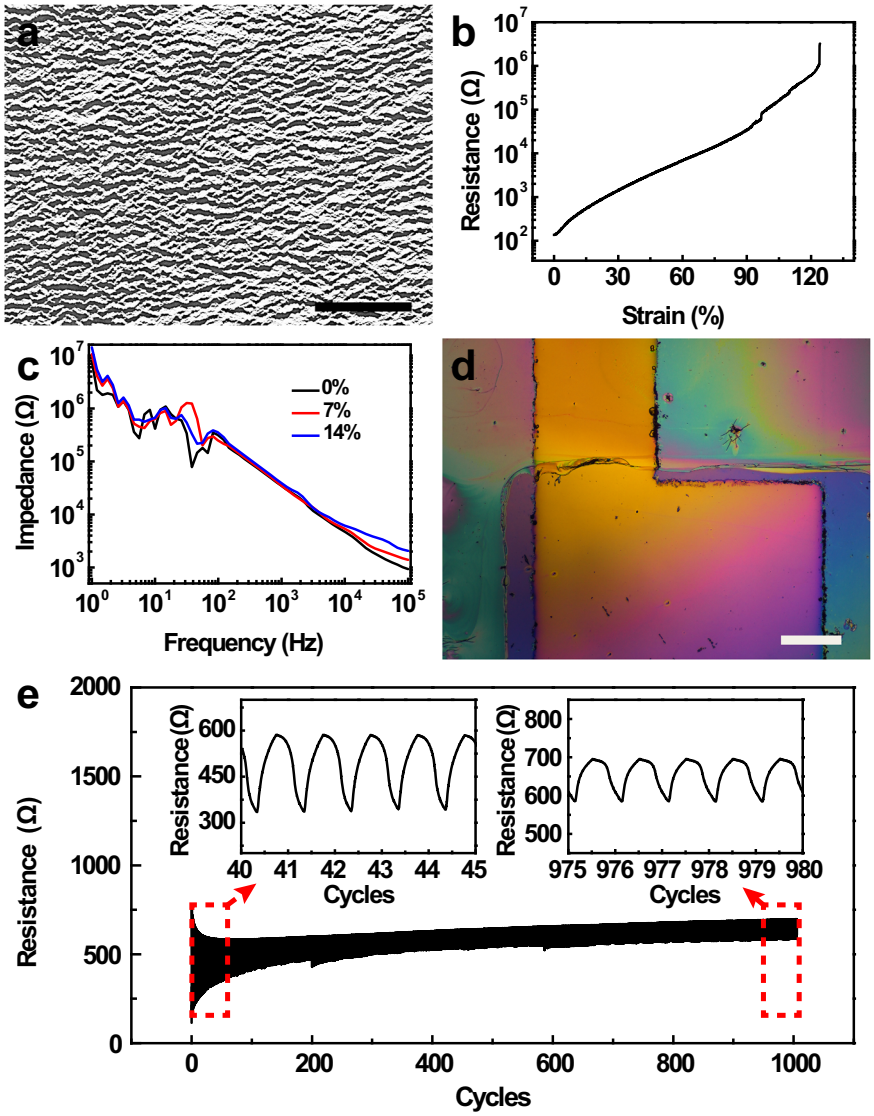

Fig. 4 Characterization of electrode. a SEM image of the electrode surface. **b** Stretchability of the electrode. **c** Impedances of the electrode under different degrees of stretching. **d** Encapsulation of the electrode. **e** Resistance change of the electrode after being stretched to 30% for 1000 cycles.

electrode (Supplementary Fig. 12). As the subject runs faster to 6 km h^{-1}, the highest acceleration is 10 g, and the electrode ability to collect EMG signals is not affected (Fig. 5g, Supplementary Movie 2). The results evidence that the SEBS-based ultrathin electrode could work properly for EMG detection in daily exercise. Unfortunately, the stretchable electrodes with thicknesses of 1 and 5 μm show obvious motion artifacts under exercising. The 90 μm-thick electrode cannot work during exercise (Supplementary Fig. 13).

In addition, human always sweat during exercise. The accumulated sweat under the EMG electrode will induce discomfort and even inflammation because of its poor water vapor permeability. Therefore, the EMG electrode with good water vapor permeability is a concern. Owing to its porosity, the as-prepared SEBS-based ultrathin porous electrode shows water vapor permeability of 25.3 g h^{-1} m^{-2} that is five times much higher than the transepidermal water loss of human skin (5−10 g h^{-1} m^{-2}). However, the water vapor permeability of the SEBS-based electrodes with thicknesses of 200 nm and 1 μm fabricated by spin coating was lower than (5−10 g h^{-1} m^{-2} (Supplementary Fig. 14a). The high water vapor permeability of the electrode offers skin comfort. After attaching our electrode on skin for 24 h, no significant inflammation is observed. But for the gel electrode, skin redness occurred after detaching it from the skin (Supplementary Fig. 14b). Furthermore, the high water vapor permeability also ensures our electrode to work properly under sweating condition. As shown in Supplementary Fig. 15, before exercise, the skin texture is clear with the SEBS-based electrodes (thicknesses of 200 nm and 1 μm). The temperature of the electrodes shows no difference (Fig. 5h). After running for 30 min, the subject sweats at a rate of 2.8 mg cm^{-2} min^{-1}. The 1 μm-thick electrode and the commercial gel electrode exhibit lower water vapor permeability than the porous 200 nm-thick electrode. After doing sports, the accumulated sweat separates the 1 μm-thick electrode from the skin, leading to skin texture disappearance. The accumulated heat will induce higher temperature on the surface of the 1 μm-thick electrode and the commercial gel electrode. However, as the sweat evaporates through the porous 200 nm-thick electrode and takes heat away, the skin texture is well-kept and the temperature of the porous 200 nm-thick electrode is the same as that of the surrounding skin. After removing these electrodes, a lower temperature of skin attaching to 1 μm-thick electrode and gel electrode than that attaching to ultrathin porous electrode is

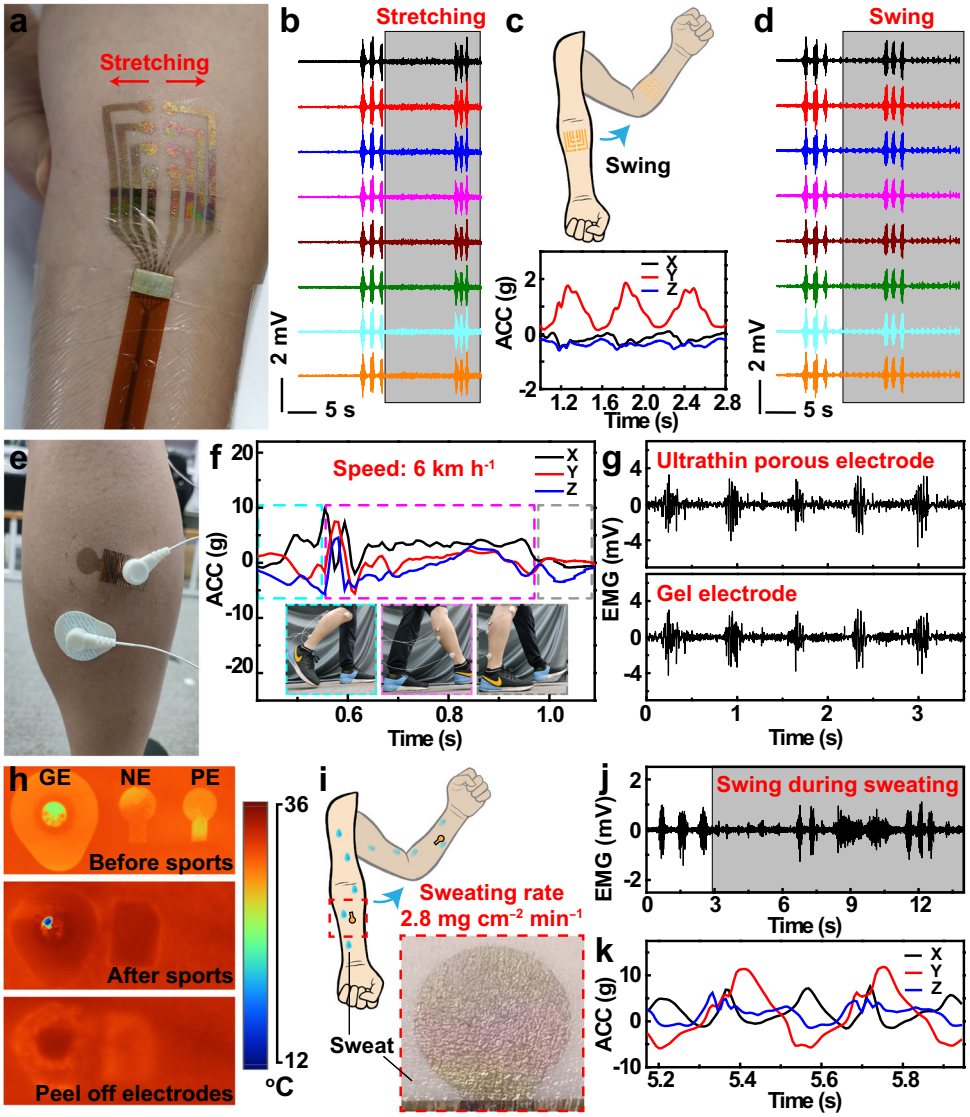

Fig. 5 EMG tests. **a** Photograph of the stretching electrode−skin interface. **b** EMG signals during the stretching process. **c** Schematic illustration showing the swinging arm and its acceleration. **d** EMG signals during the arm swinging process. **e** Photograph of the ultrathin porous electrode attached to the leg. **f** Acceleration of the leg when running at a speed of 6 km h^{-1}. **g** EMG signals detected by the SEBS-based ultrathin porous electrode and the gel electrode during running. **h** Temperature change of the gel electrode (GE), the nonporous ultrathin electrode (NE), and the porous electrode (PE) with thickness of 200 nm when doing sports. **i** Swinging arm sweats at a rate of 2.8 mg cm^{-2} min^{-1}. **j**, **k** EMG signals and acceleration of the swinging arm.

observed due to the evaporation of the accumulated sweat. This also reflects the good perspiration performance of the presented porous 200 nm-thick electrode.

During sweating, our electrode can detect EMG properly, and shows a signal to noise ratio comparable to the gel electrode. This can be attributed to the increased skin moisture (Supplementary Fig. 16). Furthermore, as the electrode attaches conformably to the skin (Fig. 5i), it shows good anti-motion artifacts. The electrode can work properly when stretching the skin dynamically from 0 to 14% (Supplementary Fig. 17) or the swinging the arm at an acceleration of 10 g under sweating condition (Fig. 5j–k, Supplementary Movie 3).

ECG and EEG recording properties of the electrode system

The ultrathin porous stretchable electrode also exhibits good performance in ECG and EEG detection. The electrode was laminated on the subject's chest of to detect ECG. As shown in Supplementary Fig. 18, P, Q, R, S, and T waves are distinguished when the subject is resting or squatting, or skin around the electrode is pressed, which suggest the electrode's comparable anti-motion artifact property to gel electrode. After running for 30 min, the subject sweated at a speed of 3.2 mg cm^{-2} min^{-1}. A lot of sweat accumulates under the medical dressing, but the skin texture is still kept with our dry electrode (Fig. 6a). Apart from this, our electrode can identify the characteristic peaks of ECG (Fig. 6b) even when the subject is squatting (Fig. 6c) or walking (Fig. 6e), or the skin nearby the electrode is pressed (Fig. 6d). As shown in Supplementary Fig. 19, the signal to noise ratio when the subject moving shows no significant change.

Because of the weak signal strength in the microvolts range, recording high-quality EEG signals is much more challenging than collecting ECG and EMG. The ultrathin porous electrode is attached to the subject's forehead to measure EEG (Supplementary Fig. 20). It shows comparable performance to gel electrode before and after sweating. During the test, one subject was asked to keep his eyes open for 20 s and then close the eyes for 20 s to

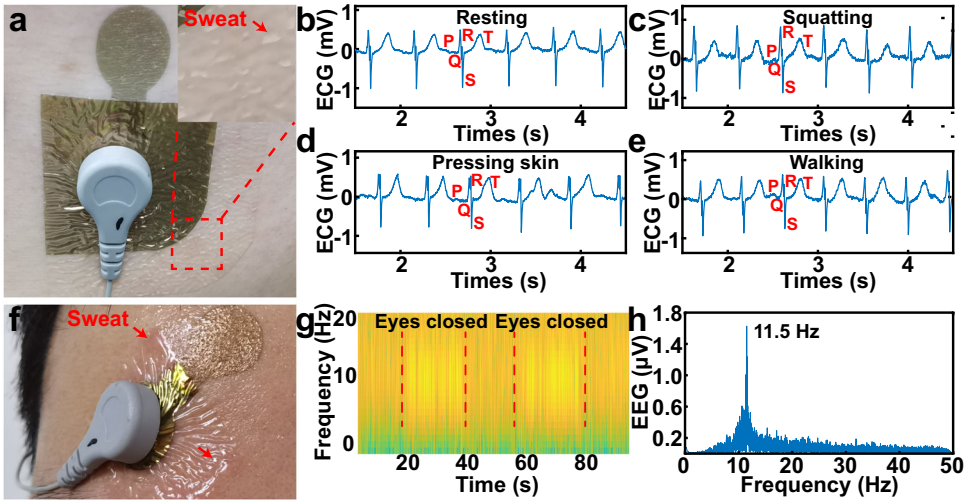

Fig. 6 ECG and EEG tests. a Photograph of the ultrathin porous electrode attached to the chest during sweating. ECG signals during resting (**b**), squatting (**c**), pressing skin (**d**), and walking (**e**) under sweating condition. **f** Photograph of the ultrathin porous electrode attached to the forehead during sweating. **g** Alpha rhythm recorded with the ultrathin porous electrode from the forehead of a volunteer during sweating. **h** Alpha rhythm centered at ~11.5 Hz.

detect the EEG signal. As shown in Supplementary Fig. 21, the alpha rhythm with frequency range of 7−15 Hz during the eye closure is acquired successfully. In contrast, when the eyes are opened, the EEG possesses a broader frequency range. After the subject was running for 30 min, a sweating rate of 2.6 mg cm^{-2} min^{-1} was observed. Sweat bag is found in Fig. 6f under the medical dressing, which has cause skin redness. However, this phenomenon did not happen on the ultrathin porous electrode due to its high water permeability. After sweating, the alpha rhythm is also acquired, indicating the good anti-perspiration property of this ultrathin porous stretchable electrode (Fig. 6g, h).

Problems to be resolved

Even though the as-prepared ultrathin porous stretchable electrode shows strenuous exercise-tolerance and good anti-perspiration properties as described above, it can be further improved. For example, the electrode with poor mechanical property is susceptible to damage upon being pressed with a high force (Supplementary Fig. 22). In addition, differences in Young's modulus between the electrode and the connecter limit its application to a certain degree. For instance, when the electrode is stretched in a direction parallel to the connecter, the strain will concentrate in the interface between them, thereby impacting its physiological electrical signal acquisition (Supplementary Movie 4).

In summary, a porous nano-thick stretchable dry electrode system was reported for the continuous multi-channel electrophysiological monitoring under strenuous exercise. It exhibits stretchability of 120% and water permeability of 25.3 g h^{-1} m^{-2}. It can be laminated conformably on the skin and stretch with it even under sweating conditions. Owing to these features, the electrode could detect EMG when the skin is stretched dynamically from 0 to 14% or under an acceleration of 10 g at a sweating rate of 2.8 mg cm^{-2} min^{-1}. Furthermore, it also shows strenuous exercise-tolerance and good anti-perspiration properties for the detection of ECG and EEG. The strategy proposed opens up the exploration of stably recording electrophysiological signals under strenuous exercise scenarios.

METHODS

Preparation and characterization of SEBS-based ultrathin porous stretchable films

SEBS (H1221, Asahi Kasei Corporation) was dissolved in toluene (AR, Shanghai Lingfeng Chemical Reagent CO., Ltd.) to achieve SEBS solutions with different concentrations. Petri dishes filled with sodium chloride solutions of different concentrations were put in a fume hood, followed by dropping 20 μL SEBS solutions with different concentrations in them. After the toluene evaporated, SEBS-based ultrathin porous stretchable films were formed on the surface of sodium chloride solutions. The toluene evaporation rate can be controlled by adjusting the wind speed in the fume hood. After that, a PET ring was attached to the surface of the film to lift it up. The thicknesses of the SEBS films were measured by the step profiler (DektakXT, Bruker). The pore size distribution of the film was counted by an optical microscope (Nikon 80i).

Preparation and characterization of SEBS-based ultrathin porous stretchable electrodes

A layer of gold was sputtered on SEBS-based ultrathin porous stretchable films to fabricate SEBS-based ultrathin porous stretchable electrodes. First, the film was attached to a silicon wafer that has a layer of sodium polystyrene sulfonate as sacrificial layer. Second, a polyethylene glycol terephthalate with special hollow structure was used as a mask to attach to the film. After that, a layer of gold was deposited on the film as conductive layer by a magnetron sputtering coating apparatus (TWS-300). The thickness of gold can be regulated through controlling the sputtering time. To encapsulate the electrodes, the sensing pad was coated with filter paper and a non-porous SEBS-based ultrathin film was coated on the film, following by removing the filter paper to expose the sensing pad. Finally, the SEBS-based ultrathin porous stretchable electrode was released from the silicon wafer by dissolving PSS in deionized water. The stretchability of the electrode was measured by using a tensile testing machine (AG-X Plus 100N) and a Keithley 2000 multimeter. The surface morphology of the electrodes was characterized by SEM (Phenom Pharos).

Measurement of the force between the electrode and the skin

The adhering force was measured using a tensile testing machine (AG-X Plus 100N). The ultrathin electrode was attached on the skin, then a PET disc with a diameter of 1 cm was attached on the electrode through double-sided adhesive. The PET was fixed on the tensile testing machine by a rope. The adhesion force was measured by pulling the PET disc until adhesion failure.

Characterization of strenuous exercise-tolerance and anti-perspiration of SEBS-based ultrathin porous stretchable electrodes

The physiological electrical signals were measured by homemade equipment. For EMG testing, the SEBS-based ultrathin porous electrode was attached to the subject's arm, gel electrodes were attached to the wrist as reference electrode and right leg drive. Then the EMG signals were measured when the skin was disturbed, such as stretching the skin dynamically from 0 to 14%, pressing the skin around the electrode, pressing the electrode, vibrating the skin, twisting the arm, swinging the arm. After that, the SEBS-based ultrathin porous electrode was attached to the subject's leg, gel electrodes were attached to the ankle as reference electrode and right leg drive. Then the EMG signals were measured when the subject was running to test the electrode's strenuous exercise-tolerance. Furthermore, the subject was asked to run at a speed of 6 km h^{-1} for 30 min at 30 °C. Then the EMG was tested when his arm was swinging or his skin was stretching to characterize the electrode's anti-perspiration property. The acceleration was measured by fixing a Trigno™ Wireless System (Delsys) on the arm or leg of the subject during movement. For ECG, the ultrathin porous electrode was attached to the subject's chest, the reference electrode was on his belly and the right leg drive was on his right leg. The ECG signals during resting, squatting, and walking slowly were detected before and during sweating. For EEG, the ultrathin porous electrode was attached to the subject's forehead, the reference electrode and right leg drive were behind the ears. Then the EEG signals before and during sweating were measured. The temperature of the electrode was detected by an infrared thermal imager (Fluke TiX580). This experiment was approved by the Human Experiment Ethics Management Committee of Shenzhen Institute of Advanced Technology, Chinese Academy of Sciences and has informed written consent from all participants. The project number was SIAT-IRB-210815-H0573.

Measurement of water vapor transmission rate

The water vapor transmission rate of electrodes at 20 °C was evaluated depending on the standard ASTM E96-95. The tests were conducted by measuring the weight loss of water in a bottle where the opening was covered by the electrode. The WVTR was calculated by the equation:

$$\mathrm{WVTR} = G/tA \quad (1)$$

where G is the weight loss, t is the time for the weight loss, and A is the test area of the electrode.

Measurement of sweat rate

After the subject was running for 30 min, square tissue was attached to the leg, chest, and forehead for 5 min to adsorb the sweat. The sweating rate was calculated from the weight change of the square tissue, as shown in the equation:

$$\mathrm{SR} = M/tA \quad (2)$$

where M is the change of weight of the tissue, t is 5 min, and A is the area of the tissue.

DATA AVAILABILITY

The data supporting the results in this study are available within the paper and its Supplementary Information. Data generated in this study, including source data and the data used to produce the figures, are available from the authors.

CODE AVAILABILITY

The codes supporting the results in this study are available within the paper and Supplementary Information.

Received: 5 April 2022; Accepted: 24 July 2022;
Published online: 18 August 2022

REFERENCES

1. Bensmaia, S. J., Tyler, D. J. & Micera, S. Restoration of sensory information via bionic hands. *Nat. Biomed. Eng.* https://doi.org/10.1038/s41551-020-00630-8 (2020).
2. Zhu, M. et al. Flexible electrodes for in vivo and in vitro electrophysiological signal recording. *Adv. Healthc. Mater.* **10**, 2100646 (2021).
3. Kuiken, T. A. et al. Targeted muscle reinnervation for real-time myoelectric control of multifunction artificial arms. *J. Am. Med. Assoc.* **301**, 619–628 (2009).
4. Liu, J. et al. Intrinsically stretchable electrode array enabled in vivo electrophysiological mapping of atrial fibrillation at cellular resolution. *Proc. Natl Acad. Sci. U.S.A.* **117**, 14769–14778 (2020).
5. Cai, Z. et al. Noninvasive high-frequency oscillations riding spikes delineates epileptogenic sources. *Proc. Natl Acad. Sci. U.S.A.* **118**, e2011130118 (2021).
6. Laffranchi, M. et al. The Hannes hand prosthesis replicates the key biological properties of the human hand. *Sci. Robot.* **5**, eabb0467 (2020).
7. Zhuang, K. Z. et al. Shared human-robot proportional control of a dexterous myoelectric prosthesis. *Nat. Mach. Intell.* **1**, 400–411 (2019).
8. Salminger, S. et al. Long-term implant of intramuscular sensors and nerve transfers for wireless control of robotic arms in above-elbow amputees. *Sci. Robot.* **4**, eaaw6306 (2019).
9. Branco, M. P., Pels, E. G. M., Nijboer, F., Ramsey, N. F. & Vansteensel, M. J. Brain-computer interfaces for communication: preferences of individuals with locked-in syndrome, caregivers and researchers. *Disabil. Rehabil-Assi.* https://doi.org/10.1080/17483107.2021.1958932 (2021).
10. Yang, J. C. et al. Electronic skin: recent progress and future prospects for skin-attachable devices for health monitoring, robotics, and prosthetics. *Adv. Mater.* **31**, 1904765 (2019).
11. Li, Q. et al. Highly thermal-wet comfortable and conformal silk-based electrodes for on-skin sensors with sweat tolerance. *ACS Nano* **15**, 9955–9966 (2021).
12. Wu, H. et al. Materials, devices, and systems of on-skin electrodes for electrophysiological monitoring and human-machine interfaces. *Adv. Sci.* **8**, 2001938 (2021).
13. Sun, Y. & Yu, X. Capacitive biopotential measurement for electrophysiological signal acquisition: a review. *IEEE Sens. J.* **16**, 2832–2853 (2016).
14. Hwang, I. et al. Multifunctional smart skin adhesive patches for advanced health care. *Adv. Healthc. Mater.* **7**, 1800275 (2018).
15. Zhao, Y. et al. Ultra-conformal skin electrodes with synergistically enhanced conductivity for long-time and low-motion artifact epidermal electrophysiology. *Nat. Commun.* **12**, 4880–4880 (2021).
16. Gogurla, N., Kim, Y., Cho, S., Kim, J. & Kim, S. Multifunctional and ultrathin electronic tattoo for on-skin diagnostic and therapeutic applications. *Adv. Mater.* **33**, 2008308 (2021).
17. Zhang, L. et al. Fully organic compliant dry electrodes self-adhesive to skin for long-term motion-robust epidermal biopotential monitoring. *Nat. Commun.* **11**, 4683 (2020).
18. Wang, Y. et al. Electrically compensated, tattoo-like electrodes for epidermal electrophysiology at scale. *Sci. Adv.* **6**, eabd0996 (2020).
19. Brown, M. S. et al. Electronic-ECM: a permeable microporous elastomer for an advanced bio-integrated continuous sensing platform. *Adv. Mater. Technol.* **5**, 2000242 (2020).
20. Liu, L. et al. Nanofiber-reinforced silver nanowires network as a robust, ultrathin, and conformable epidermal electrode for ambulatory monitoring of physiological signals. *Small* **15**, 1900755 (2019).
21. Wang, Y. et al. Low-cost, mu m-thick, tape-free electronic tattoo sensors with minimized motion and sweat artifacts. *npj Flex. Electron* **2**, 6 (2018).
22. Stauffer, F. et al. Skin conformal polymer electrodes for clinical ECG and EEG recordings. *Adv. Healthc. Mater.* **7**, 1700994 (2018).
23. Ameri, S. K. et al. Graphene electronic tattoo sensors. *ACS Nano* **11**, 7634–7641 (2017).
24. Fang, Y. et al. Solution-processed submicron free-standing, conformal, transparent, breathable epidermal electrodes. *ACS Appl. Mater. Interfaces* **12**, 23689–23696 (2020).
25. Fang, Y. et al. Cryo-transferred ultrathin and stretchable epidermal electrodes. *Small* **16**, 2000450 (2020).
26. Ferrari, L. M. et al. Ultraconformable temporary tattoo electrodes for electrophysiology. *Adv. Sci.* **5**, 1700771 (2018).
27. Miyamoto, A. et al. Inflammation-free, gas-permeable, lightweight, stretchable on-skin electronics with nanomeshes. *Nat. Nanotechnol.* **12**, 907–913 (2017).
28. Yang, X. et al. Ultrathin, stretchable, and breathable epidermal electronics based on a facile bubble blowing method. *Adv. Electron. Mater.* **6**, 2000306 (2020).
29. Wang, Y. et al. Robust, self-adhesive, reinforced polymeric nanofilms enabling gas-permeable dry electrodes for long-term application. *Proc. Natl Acad. Sci. U. S. A.* **118**, e2111904118 (2021).
30. Nawrocki, R. A. et al. Self-adhesive and ultra-conformable, sub-300 nm dry thin-film electrodes for surface monitoring of biopotentials. *Adv. Funct. Mater.* **28**, 1803279 (2018).
31. Kim, T., Park, J., Sohn, J., Cho, D. & Jeon, S. Bioinspired, highly stretchable, and conductive dry adhesives based on 1D-2D hybrid carbon nanocomposites for all-in-one ECG electrodes. *ACS Nano* **10**, 4770–4778 (2016).

32. Ershad, F. et al. Ultra-conformal drawn-on-skin electronics for multifunctional motion artifact-free sensing and point-of-care treatment. *Nat. Commun.* **11**, 3823 (2020).
33. Zhou, W. et al. Gas-permeable, ultrathin, stretchable epidermal electronics with porous electrodes. *ACS Nano* **14**, 5798–5805 (2020).
34. Xu, Y. et al. Multiscale porous elastomer substrates for multifunctional on-skin electronics with passive-cooling capabilities. *Proc. Natl Acad. Sci. U.S.A.* **117**, 205–213 (2020).
35. Sun, B. et al. Gas-permeable, multifunctional on-skin electronics based on laser-induced porous graphene and sugar-templated elastomer sponges. *Adv. Mater.* **30**, 1804327 (2018).
36. Zhang, B. et al. Stretchable conductive fibers based on a cracking control strategy for wearable electronics. *Adv. Funct. Mater.* **28**, 1801683 (2018).
37. Li, Q. & Tao, X. M. Three-dimensionally deformable, highly stretchable, permeable, durable and washable fabric circuit boards. *P. Roy. Soc. A-Math. Phy.* **470**, 20140472 (2014).
38. Jeong, W. et al. All-organic, solution-processed, extremely conformal, mechanically biocompatible, and breathable epidermal electrodes. *ACS Appl. Mater. Interfaces* **13**, 5660–5667 (2021).
39. Ma, Z. et al. Permeable superelastic liquid-metal fibre mat enables biocompatible and monolithic stretchable electronics. *Nat. Mater.* **20**, 859–868 (2021).
40. Yang, H. et al. Adhesive biocomposite electrodes on sweaty skin for long-term continuous electrophysiological monitoring. *ACS Mater. Lett.* **2**, 478–484 (2020).
41. Fedorchenko, A. I. & Hruby, J. On formation of dry spots in heated liquid films. *Phys. Fluids* **33**, 023601 (2021).
42. Scriven, L. E. & Sternling, C. V. Marangoni effects. *Nature* **187**, 186–188 (1960).
43. Chun, S. et al. Conductive and stretchable adhesive electronics with miniaturized octopus-like suckers against dry/wet skin for biosignal monitoring. *Adv. Funct. Mater.* **28**, 1805224 (2018).
44. Drotlef, D.-M., Amjadi, M., Yunusa, M. & Sitti, M. Bioinspired composite microfibers for skin adhesion and signal amplification of wearable sensors. *Adv. Mater.* **29**, 1701353 (2017).
45. Kwak, M. K., Jeong, H.-E. & Suh, K. Y. Rational design and enhanced biocompatibility of a dry adhesive medical skin patch. *Adv. Mater.* **23**, 3949–3953 (2011).
46. Chun, S. et al. Water-resistant and skin-adhesive wearable electronics using graphene fabric sensor with octopus-inspired microsuckers. *ACS Appl. Mater. Interfaces* **11**, 16951–16957 (2019).
47. Shahrizaila, N. Non-invasive electromyography as a disease biomarker: are we only scratching the surface? *Clin. Neurophysiol.* **132**, 808–809 (2021).
48. Noto, Y.-I. et al. High-density surface electromyography to assess motor unit firing rate in Charcot-Marie-Tooth disease type 1A patients. *Clin. Neurophysiol.* **132**, 812–818 (2021).

ACKNOWLEDGEMENTS

This work was supported by China Postdoctoral Science Foundation (2021M693317), the National Natural Science Foundation of China under Grant (62101545, 81927804, U1913601, 62003331), Guangdong-Hong Kong-Macao Joint Laboratory of Human-Machine Intelligence-Synergy Systems (2019B121205007), the NSFC-Shenzhen Robotics Basic Research Center Program (U2013207), the Natural Science Foundation of Guangdong Province (2018A030313065), the National Key Research and Development Project, MOST (2020YFC2005803), GuangDong Basic and Applied Basic Research Foundation (2020A1515110205).

AUTHOR CONTRIBUTIONS

R.X. designed the research and performed the experiments. Q.L., Z.C., F.H., Q.T., J.S., Y.Z., M.Y., D.Q., and P.G. helped collect data. L.T. assisted in drawing illustrations. G.L. and F.H. supervised the project. Z.L. supervised the project, helped design the experiments, and revised the manuscript.

COMPETING INTERESTS

The authors declare no competing interests.

ADDITIONAL INFORMATION

Supplementary information The online version contains supplementary material available at https://doi.org/10.1038/s41528-022-00209-0.

Correspondence and requests for materials should be addressed to Guanglin Li, Fengwei Huo or Zhiyuan Liu.